Analytical and experimental comparisons between the frequency-modulated–frequency-shift measurement and the pulsed-wave–time-shift measurement Doppler systems

Wilhjelm, Jens E.; Pedersen, P. C.

Published in:
Acoustical Society of America. Journal

Link to article, DOI:
10.1121/1.417214

Publication date:
1996

Document Version
Publisher's PDF, also known as Version of record

Analytical and experimental comparisons between the frequency-modulated–frequency-shift measurement and the pulsed-wave–time-shift measurement Doppler systems

Jens E. Wilhjelm[a)]
Department of Information Technology, Technical University of Denmark, Building 344, DK-2800 Lyngby, Denmark

Peder C. Pedersen[b)]
Electrical and Computer Engineering Department, Worcester Polytechnic Institute, Worcester, Massachusetts 01609

(Received 7 March 1995; accepted for publication 25 July 1996)

In previous publications, a new echo-ranging Doppler system based on transmission of repetitive coherent frequency-modulated (FM) sinusoids in two different implementations was presented. One of these implementations, the frequency-modulated–frequency-shift measurement (FM–fsm) Doppler system is, in this paper, compared with its pulsed-wave counterpart, the pulsed-wave–time-shift measurement (PW–tsm) Doppler system. When using transmitted PW and FM signals with a Gaussian envelope, the parallelism between the two systems can be stated explicitly and comparison can be made between the main performance indices for the two Doppler systems. The performance of the FM and PW Doppler systems is evaluated by means of numerical simulation and measurements of actual flow profiles. The results indicate that the two Doppler systems have very similar levels of performance. © *1996 Acoustical Society of America.*

PACS numbers: 43.80.Vj [FD]

LIST OF SYMBOLS

B_0	$=f_2-f_1$, frequency excursion of transmitted signal
B_{rms}	rms bandwidth of transmitted signal
D	nominal range
ΔD	axial range cell distance defined by signal processing
$d^{(n)}$	$=d^{(0)}+\nu n T_r$, range of scatterer at the onset of nth transmission
f_0	center frequency of transmitted signal; for FM: $f_0=(f_1+f_2)/2$
f_1	''start'' instantaneous frequency of transmitted sweep signal ($@t=0$)
f_2	''stop'' instantaneous frequency of transmitted sweep signal ($@t=t_m$)
Δf_a	$=\tau_0 S_0$, change in position frequency between two consecutive fsm spectra
$f_a^{(n)}$	$=(t^{(n)}-t_s)S_0$, position (or center) frequency of the fsm spectrum
f_w	$=(2\Delta D/c)S_0$, width of spectral window in fsm signal processing
S_0	$=B_0/t_m$, sweep rate of transmitted FM signal
$t^{(n)}$	$=2d^{(n)}/c$, ultrasound round trip travel time for scatterer at the onset of transmission number n
$t_a^{(n)}$	measure of rate of oscillations of the nth spectral cross-correlation function in the FM–fsm Doppler system
$t_d^{(n)}$	$=t^{(n)}-t$, difference between acoustic delay ($t^{(n)}$) and system delay (t_s)
t_m	time duration of transmitted signal
T_r	pulse or sweep repetition time
t_s	$=2D/c$, time delay corresponding to nominal range
T_w	$=2\Delta D/c$, duration of time window in tsm signal processing
ν	velocity component of target (scatterer) along ultrasound beam
ν_{alias}	aliasing velocity in a psm Doppler system
α	form factor for Gaussian envelope
α_G	$=2(\alpha/t_m)^2$, combined form factor
β	$=(c-\nu)/(c+\nu)$, Doppler compression factor
γ	frequency shift in cross-correlation function
τ_0	$=2\nu T_r/c$, change in round-trip travel time between consecutive received signals

INTRODUCTION

The noninvasive assessment of blood flow with Doppler ultrasound is, today, a standard technique in hospitals and clinics. It is used extensively for studying cardiac hemodynamics and the flow pattern in arteries and veins (e.g., carotid artery). The prevailing technique is PW (pulsed-wave) Doppler in which a series of short bursts of ultrasound energy is transmitted. From the Doppler compression of the backscattered signal from the moving red blood cells, the velocity of the blood can be estimated. This may be done with either the conventional[1–3] technique, based on *phase-shift measurement* (PW–psm[4]) or with a newer technique, utilizing *time-shift measurement* (PW–tsm).[4–8]

However, the use of sound bursts of short time duration results in a high peak transmitted power. To reduce this, but

[a)]Electronic mail: wilhjelm@it.dtu.dk
[b)]Electronic mail: pedersen@ee.wpi.edu

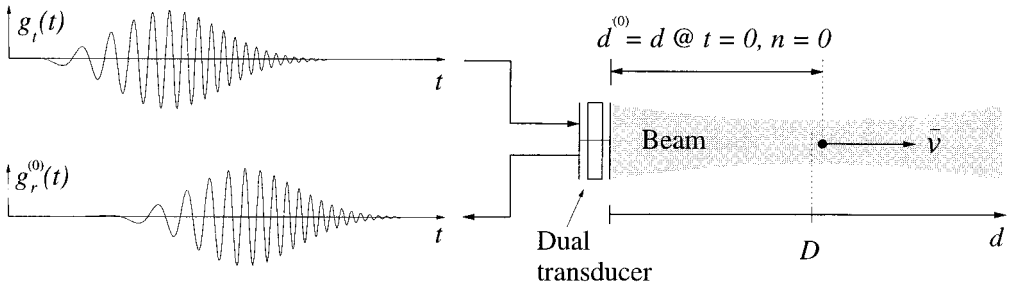

FIG. 1. Sketch of idealized measurement situation. A single scatterer is moving with velocity, v, axially along the axis of the transmitted beam in the direction away from the transducer. It is located at range $d^{(0)}$ at $t=0$ and $n=0$. The nominal range, D, will be introduced in Sec. III. To the left, one transmitted signal with the corresponding received signal is shown.

at the same time maintain the wide bandwidth of the transmitted signal, several types of coded transmission signals have been devised, such as *random noise*[9,10] and *pseudorandom noise*.[11,12] A common element in these approaches is the use of *phase-shift measurements* in the signal processing. In contrast, the Doppler system presented here utilizes coherent, repetitive frequency-modulated (FM) signals as transmission signals where the velocity information may be extracted either with phase shift measurement (FM–psm) or frequency-shift measurement (FM–fsm).[13,14] The signal theory and systems description for these two versions of the FM Doppler system were presented in two previous papers.[14,15] It was shown that the FM–psm and FM–fsm Doppler techniques in several respects are analogous to the PW–psm and PW–tsm techniques, respectively. Simultaneous transmission and reception is generally utilized in the FM Doppler system, thus requiring a dual transducer system.

In this paper, the FM–fsm technique will be contrasted analytically and experimentally with the PW–tsm technique, as FM–fsm appears to offer unique advantages over FM–psm, such as reduced influence of medium attenuation. In addition, the PW–tsm and FM–fsm techniques have the potential of avoiding the velocity aliasing phenomena, known from psm signal processing. By weighting the transmitted signals with a Gaussian envelope, closed form expressions are obtainable for the relevant signals, spectra, and cross-correlation functions for both FM–fsm and PW–tsm. Furthermore, the Gaussian envelope gives a fairly realistic representation of the electro-acoustic transfer function of actual broadband transducers. Exploiting the parallelism between the FM–fsm and the PW–tsm Doppler systems, it is shown that the two main performance indices (range cell size and accuracy in the velocity estimation) are comparable.

The paper contains the following parts: In Sec. I, the mathematical expressions for the transmitted signal for both FM and PW Doppler systems are stated together with expressions for the rms bandwidth. In Sec. II, the received signal for a single scatterer is given, and the FM-fsm Doppler system is analyzed and contrasted with the PW–tsm Doppler system in Sec. III. Section IV describes the parallels between the two systems and argues that the performance indices are roughly identical. Finally, simulation results and experimental results are presented in Secs. V and VI, respectively.

I. THE TRANSMITTED SIGNAL

The transmitted signal for the FM Doppler system consists of a series of linearly frequency-modulated sinusoids (sweeps) with a Gaussian envelope function that is truncated to be zero outside the interval $[0;t_m]$. Specifically, a sweep of duration t_m seconds is transmitted every T_r seconds ($T_r > t_m$); T_r is thus the sweep repetition time. The entire transmitted signal consists of a total of L individual sweep signals, labeled 0 to $L-1$. A given transmitted signal and corresponding received signal are denoted by the superscript$^{(n)}$, but as all the individual transmitted sweeps are identical, the n notation is only used for the received signals. In the following derivations, local time—denoted t—is used, which means that $t=0$ at the onset of each transmitted sweep. The transmitted signal for the PW Doppler system consists of a corresponding series of short duration bursts, also with a Gaussian envelope, with a burst interval of T_r seconds.

For the purpose of deriving analytic solutions to the signals and parameters, generated by the signal processing of the received signals, Gaussian enveloped signals extending over the interval $]-\infty;\infty[$ will be used, so that one transmitted signal can be expressed in the following form:

$$g_t(t) = \mathrm{Re}\{\tilde{g}_t(t)\} = \mathrm{Re}\left\{ \exp\left[-2\left(\frac{\alpha}{t_m}\right)^2 \left(t - \frac{t_m}{2}\right)^2 \right] \times \exp[j(2\pi f_1 t + \pi S_0 t^2)] \right\}, \quad (1)$$

where tilde ($\tilde{\ }$) denotes complex variables and Re { } extracts the real part. An example of this signal is shown in Fig. 1. In (1), t_m is the *time duration* of the truncated sweep signal used in the actual implementation. If $\alpha=3$, then the value of the envelope function at $t=0$ and $t=t_m$ will be $\cong 1.1\%$ of the maximum value obtained at $t=t_m/2$. This α value is also used by Harris.[16] With an appropriate choice of α, such as the one used above, the difference between $g_t(t)$, as given in (1), and the truncated $g_t(t)$, used in the actual measurement system, is negligible. The analytical results will be derived from the untruncated $g_t(t)$ where it is assumed that each set of transmitted and received signals is unaffected by the $L-1$ other sets. For the complex version of the sweep signal, $\tilde{g}_t(t)$, it is seen that the instantaneous frequency at $t=0$ is f_1 and the instantaneous frequency at $t=t_m$

is $f_2=f_1+S_0t_m$. These two frequencies are hereafter called *start* and *stop* frequencies, respectively, as they indicate the sweep range in a physical system. The *frequency excursion*, produced during t_m, is thus $B_0=f_2-f_1$. The center frequency of the spectrum of the signal in (1) is $f_0=(f_1+f_2)/2$ which, in general, is assumed to be equal to the center frequency of the transducer. It is finally noted that a PW excitation signal can be obtained from (1) by setting $S_0=0$, replacing f_1 with f_0 and using a much smaller t_m value, chosen to match the PW bandwidth with that of the sweep signal.

The magnitude spectrum of a signal with a Gaussian envelope is Gaussian as well.[17] The rms bandwidth[17,18] in Hz of $\tilde{g}_t(t)$, as given in (1), can be found to be[18]

$$B_{\mathrm{FM,rms}}=\sqrt{\frac{\int_{-\infty}^{\infty} f^2|\tilde{G}_t(f)|^2\,df}{\int_{-\infty}^{\infty}|\tilde{G}_t(f)|^2\,df}}=\sqrt{\frac{B_0^2}{8\alpha^2}+\frac{\alpha^2}{2\pi^2t_{m,\mathrm{FM}}^2}}, \tag{2}$$

where $\tilde{G}_t(f)$ is the spectrum of $\tilde{g}_t(t)$. It is seen that the bandwidth expression combines contributions from both the signal parameters, t_m and α, and from the frequency excursion, B_0.

From (2), it is seen that the rms bandwidth of a transmitted PW signal ($B_0=0$) is

$$B_{\mathrm{PW,rms}}=\frac{1}{\sqrt{2}\pi}\,\frac{\alpha}{t_{m,\mathrm{PW}}}=\frac{1}{4\pi}\,\frac{1}{t_{m,\mathrm{PW,rms}}}, \tag{3}$$

where $t_{m,\mathrm{PW}}$ is the duration of the transmitted PW burst and $t_{m,\mathrm{PW,rms}}=t_{m,\mathrm{PW}}/(\sqrt{8}\alpha)$ is the corresponding rms duration.[18] To make a valid comparison between the two Doppler techniques, the operating conditions must be identical, which, among other things, requires the same bandwidth of the transmitted signals. Thus applying $B_{\mathrm{FM,rms}}=B_{\mathrm{PW,rms}}$ to (2) and (3) yields

$$\frac{1}{t_{m,\mathrm{PW}}^2}=\frac{\pi^2}{4\alpha^4}\,B_0^2+\frac{1}{t_{m,\mathrm{FM}}^2}, \tag{4}$$

where α is assumed identical for the two systems and $t_{m,\mathrm{PW}}$ and $t_{m,\mathrm{FM}}$ are the lengths of the transmitted PW and FM signals, respectively. For the case when

$$\frac{\pi^2}{4\alpha^4}\,B_0^2\gg\frac{1}{t_{m,\mathrm{FM}}^2}, \tag{5}$$

i.e., the contribution from B_0 dominates, (4) simplifies to

$$t_{m,\mathrm{PW}}=\frac{2\alpha^2}{\pi B_0}. \tag{6}$$

Thus t_m for the PW Doppler system will be determined from α and the chosen frequency excursion, B_0, for the corresponding FM Doppler system. It is assumed throughout the paper that (5) is fulfilled and (6), therefore, is valid.

II. THE RECEIVED SIGNAL

The received signal, based on the excitation in (1), will now be found for the idealized measurement situation illustrated in Fig. 1. A single scatterer, with a frequency-independent backscattering coefficient r, is moving axially away from the transducer with velocity v. The term *backscattering coefficient* is here chosen to mean the ratio of the transmitted pressure amplitude (plane wave) to the received pressure amplitude, at the location of the receiving transducer. As shown in Fig. 1, the range of the particle is $d^{(0)}$ at $t=0$ and $n=0$. The propagation speed of sound in the medium between the particle and transducer is c, and the medium is assumed to be perfectly elastic. The scatterer is assumed insonified with a plane-wave pressure field from the transducer, the time dependence of which is described by (1). For the signal analysis performed here, the bandlimited signal, $g_t(t)$, is applied to the transducer which is assumed to have a flat frequency response. In contrast, a constant amplitude sweep signal is applied in the physical implementation where the shaping of the envelope of the received signal—in the paper assumed to be Gaussian—is introduced by the bandlimited frequency response of the transducer. Under the given assumptions, the nth received signal is a time-shifted and Doppler-compressed replica of the nth transmitted signal[15]

$$g_r^{(n)}(t)=rg_t\left[\beta\left(t-2\frac{d^{(n)}}{c-\nu}\right)\right], \tag{7}$$

where $\beta=(c-\nu)/(c+\nu)$ (β is the reciprocal of the β defined in Ref. 15) is the Doppler compression factor, and $d^{(n)}=d^{(0)}+\nu nT_r$ describes the range of the scatterer at the onset of the nth transmission. Applying (1) to (7) yields the received signal, $g_r^{(n)}(t)$, where it is assumed that $g_t(t)$ in (1) only exists in the time interval $0\leqslant t\leqslant t_m$:

$$\begin{aligned}g_r^{(n)}(t)=\mathrm{Re}\Bigg(r\,\exp\Bigg[-\alpha_G\left(\beta t-2\frac{\beta d^{(n)}}{c-\nu}-\frac{t_m}{2}\right)^2\Bigg]\\ \times\exp\Bigg\{j\Bigg[2\pi f_1\beta\left(t-\frac{2d^{(n)}}{c-\nu}\right)+\pi S_0\beta^2\\ \times\left(t-\frac{2d^{(n)}}{c-\nu}\right)^2\Bigg]\Bigg\}\Bigg),\\ \frac{2d^{(n)}}{c-\nu}\leqslant t\leqslant\frac{2d^{(n)}}{c-\nu}+\frac{t_m}{\beta},\end{aligned} \tag{8}$$

where the bounds for the time duration is given in the last line of (8). Outside this time interval, $g_r^{(n)}(t)$ is zero. Note that $\alpha_G=2(\alpha/t_m)^2$ has been introduced to simplify the notation. When comparing (1) with (8), two distinct effects are seen. First, the received signal is expanded (or compressed when ν is negative) so that its duration is t_m/β. Due to this expansion (or compression), the start frequency and the sweep rate have been Doppler shifted as well. These effects have been analyzed elsewhere.[19] The second effect that can be noted from (8) is that the arrival time of the received signals occurs with an increasing delay, relative to transmission, as the particle moves away. This corresponds to the Doppler shift of the sweep (burst) repetition time, so that the new sweep (burst) repetition time is $T_r'=T_r/\beta$. For the single scatterer, it is this effect that is measured with the PW and FM Doppler systems, considered here.[14,15] In the case of

multiple scatterers moving with a uniform velocity, this effect is observed as a *shift in the signature of consecutive received signals*. Ignoring the Doppler expansion (or compression) of the individual signals, i.e., setting $\beta=1$ and linearizing so that $c-\nu\cong c$, (8) can be written as

$$g_r^{(n)}(t)\cong \mathrm{Re}\{r\ \exp[-\alpha_G(t-t^{(n)}-t_m/2)^2] \times \exp[j(2\pi f_1(t-t^{(n)})+\pi S_0(t-t^{(n)})^2)]\},$$
$$t^{(n)}\leqslant t\leqslant t^{(n)}+t_m, \tag{9}$$

where

$$t^{(n)}=\frac{2d^{(n)}}{c}=2\,\frac{d^{(0)}+n\nu T_r}{c}=\frac{2d^{(0)}}{c}+n\tau_0. \tag{10}$$

In (10), $\tau_0 = T_r - T_r' = (2\nu/c)T_r$ represents the change in round-trip travel time between consecutive sweeps.

Finally, consider the situation in which a large, but finite number, q, of scatterers moving with the same velocity are present in the ultrasound beam. In this case we assume that the total received signal can be written as a summation of individual received signals given in (9), i.e., no multiple scattering is considered. The total received signal is

$$g_R^{(n)}(t)=\sum_{i=0}^{q-1} g_{r,i}^{(n)}(t), \tag{11}$$

where a backscattering coefficient r_i and an initial range $d_i^{(0)}$ is associated with the ith scatterer. The subscript R is employed to distinguish $g_R^{(n)}(t)$ from the received signal due to one scatterer, $g_r^{(n)}(t)$. Note that the model assumes some idealizations of the physical reality which increase the correlation between consecutive received signals and thus improves the performance. The most significant of the excluded effects are *lateral variation in ultrasound beam intensity* and *velocity variation within the range cell*. Nor does the model take into account the frequency-dependent attenuation in the medium.

It is thus assumed that the received signal from blood can be modeled as a summation of the contributions from a large number of such scatterers located randomly within a plane. Even though the analysis of the Doppler systems to follow will be based on one scatterer, the multiscatterer situation can quite easily be obtained by the use of the principle of superposition.

III. FM–fsm SIGNAL PROCESSING

In this section the FM–fsm signal processing is developed and contrasted with the PW–tsm method. First, a short description of the PW–tsm method is given.

The block diagram for the PW–tsm system is displayed in Fig. 2 with the switch in PW position. A burst generator and power amplifier generate the transmitted signal which is applied to the single crystal transducer via the transmit/receive switch. Consider the transmitted signal to be a short burst as described by (1) with $S_0=0$, $f_1=f_2=f_0$, and t_m equal to a few cycles at f_0, as specified in (6). The received signal can be bandpass filtered, to remove noise lying outside the spectral range of the signal. Following that, a segment of the received signal is extracted with the range gate window

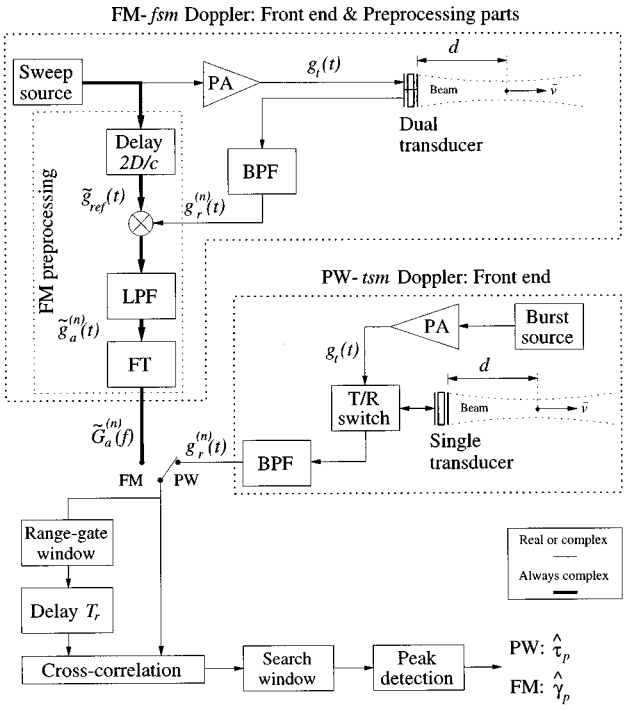

FIG. 2. Block diagram of PW–tsm and FM–fsm signal processing. With the actual switch setting, the system functions as a PW–tsm Doppler system. $\hat{\tau}_p$ and $\hat{\gamma}_p$ denote the estimated location of the global peak of the cross-correlation function, within the search window, from which the velocity is estimated.

(length T_w), delayed by T_r seconds and cross-correlated with the subsequent received signal. A search window is next applied to the cross-correlation function, and from the location of the peak inside this search window, the target velocity can be calculated. The width of the search window corresponds to one cycle of f_0 with the effect that, with a high probability, only one peak can be found inside the search window. This minimizes the possibilities for detecting a sidelobe in the cross-correlation function, but the velocity range will be restricted to $[-\nu_{\text{alias}};\ \nu_{\text{alias}}]$, where $\nu_{\text{alias}}=c/(4f_0T_r)$ is the aliasing velocity for a psm Doppler system. The actual axial resolution distance for this system is determined by contributions from both $\Delta D_{\text{PW}}=cT_w/2$ and the *minimum obtainable axial range resolution distance*, $\Delta D_{\min}=c/(2B)$, where B is the bandwidth of the transmitted signal.

The FM–fsm signal processing utilizes cross-correlation of real spectra for extracting velocity information, in a fashion quite similar to the cross-correlation of real time signals in the PW–tsm Doppler system. In previous publications,[14,15] a simpler version of the FM–fsm Doppler system was presented, based on the cross correlation of magnitude spectra. Greater precision is obtainable with cross correlation of real spectra, due to the more narrow peak in the cross-correlation function. The received signal in the FM–fsm Doppler system is basically a linear sweep signal which must be preprocessed in order to establish a unique range-frequency relationship analogous to the range–time relationship known from PW excitation. The FM–fsm preprocessing is similar to what is done in *time delay spectrometry* (TDS).[19]

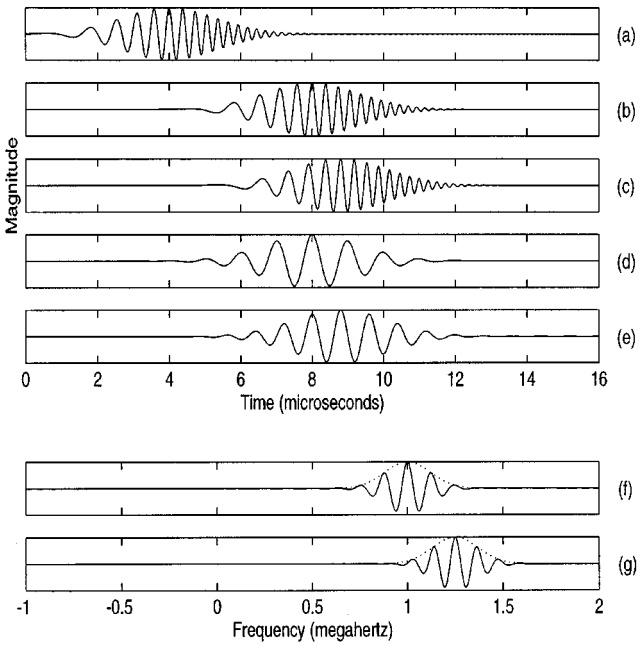

FIG. 3. Signals and spectra of the FM–fsm Doppler system. (a) Transmitted signal, $g_t(t)$. (b) and (c) First and second received signals, $g_r^{(1)}(t)$ and $g_r^{(2)}(t)$, respectively. (d) and (e) First and second demodulated signals, $g_a^{(1)}(t)$ and $g_a^{(2)}(t)$, respectively. Note that $g_a^{(2)}(t)$ is further delayed than $g_a^{(1)}(t)$ and that the mean frequency of $g_a^{(2)}(t)$ is higher than that of $g_a^{(1)}(t)$. (f) and (g) Real part (———) and magnitude (···) of first and second fsm spectra, $G_a^{(1)}(f)$ and $G_a^{(2)}(f)$, respectively. Note that these spectra oscillate at different rates and occupy different frequency ranges. The parameters are: f_0=5 MHz, B_0=5 MHz, $t_m=40/f_0$, $\alpha_G=2(3/t_m)^2$, $f_s=20f_0$. The ordinate is a relative scale from -1 to 1.

Specifically, in the preprocessing, a given received sweep signal is demodulated by using a reference sweep, and the demodulated signal is subsequently transformed into the frequency domain. The resulting spectrum is called the fsm spectrum.[14] This fsm spectrum, as will be shown later, is analogous to the received signal due to PW excitation and is processed in roughly the same fashion. The transmitted signal is given in (1) where t_m is much longer than for PW; typical values range from 50 to 200 μs. The following analysis is based on one scatterer (moving axially away from the transducer with the velocity v, as illustrated in Fig. 1).

A. FM-fsm preprocessing

The first step of the preprocessing consists of quadrature demodulation of the received sweep signals as shown in the block diagram in Fig. 2. A numeric example of the transmitted sweep signal is illustrated in Fig. 3(a), while two consecutive received signals from one moving particle are shown in Fig. 3(b) and (c). The quadrature demodulation is done by multiplying each received signal with the following reference signal which is a delayed analytic version of the transmitted signal, except that the amplitude is constant, not Gaussian:

$$\tilde{g}_{\text{ref}}(t)=\exp[j(2\pi f_1(t-t_s)+\pi S_0(t-t_s)^2)],\quad -\infty<t<\infty, \tag{12}$$

where $t_s=2D/c$ and D is the *nominal range* or *range of interest*. The multiplier output is filtered with an ideal low-pass filter (LP) with gain 2, for the purpose of eliminating the sum frequencies generated by the multiplication. The output of the filter is called $\tilde{g}_a^{(n)}(t)$. Thus

$$\tilde{g}_a^{(n)}(t)=2\text{LP}\{g_r^{(n)}(t)\tilde{g}_{\text{ref}}(t)\}. \tag{13}$$

For a single particle, the demodulated signal is a tone burst with Gaussian envelope and duration t_m. The mean frequency of this tone burst is proportional to the axial displacement of the particle from D.[15] Two consecutive demodulated signals are shown in Fig. 3(d) and (e). Next, in the second step of the preprocessing, the demodulated signal is Fourier transformed into the frequency domain, with a temporal zero reference of $t=t_s$. The resulting spectrum, $\tilde{G}_a^{(n)}(f)$, is called the *fsm spectrum*.[14] Figure 3(f) and (g) show the real and magnitude parts of two consecutive fsm spectra. As will be shown, consecutive fsm magnitude spectra are identical in shape, but shifted in frequency. The phase function changes from one fsm spectrum to the next, causing the real part of consecutive fsm spectra to differ both in frequency and in shape of the spectral waveform. The derivation of $\tilde{G}_a^{(n)}(f)$ is given in Appendix A with the following result:

$$\tilde{G}_a^{(n)}(f)=r\sqrt{\frac{\pi}{\alpha_G}}\exp\left[-\frac{\pi^2}{\alpha_G}(f_a^{(n)}-f)^2\right]\times\exp\left[j2\pi\left(t_d^{(n)}+\frac{t_m}{2}\right)(f_a^{(n)}-f)+j\varphi_b^{(n)}\right], \tag{14}$$

where

$$t_d^{(n)}=t^{(n)}-t_s,\qquad f_a^{(n)}=t_d^{(n)}S_0=(t^{(n)}-t_s)S_0=\frac{2(d^{(n)}-D)}{c}S_0, \tag{15}$$

and

$$\varphi_b^{(n)}=\pi t_d^{(n)}(2f_1-S_0t_d^{(n)}). \tag{16}$$

The frequency value, $f_a^{(n)}$, defined in (15), is called the *position frequency*[15] of the fsm spectrum. This frequency is proportional to the difference between the actual range of the particle, $d^{(n)}$, and the nominal range, D.

When the FM Doppler system is implemented to provide a velocity profile, the velocity for a set of nominal ranges, D_i, must be found. In the implementation presented in this paper, each range must be treated individually, requiring a new D *and* FT per velocity estimate or range cell. More efficient approaches can be envisioned, but these are beyond the scope of this paper.

B. Determination of the spectral cross-correlation function

When $\tilde{G}_a^{(n)}(f)$ in (14) has been obtained from the received signal, the preprocessing is completed. Further processing is done along the same lines as for the PW–tsm Doppler system: A segment around $f=0$ of width f_w is isolated from the fsm spectrum, $\tilde{G}_a^{(n)}(f)$, and then cross correlated with the subsequent fsm spectrum, $\tilde{G}_a^{(n+1)}(f)$. Different components of $\tilde{G}_a^{(n)}(f)$ and $\tilde{G}_a^{(n+1)}(f)$ may be chosen

for the cross-correlation. In our previous papers (Refs. 14 and 15), only the cross-correlation of the spectral magnitude was considered, whereas—as will be described—the emphasis in this paper is on cross correlation of the real components of the spectra. From the location of the peak in the cross-correlation function, the velocity in the range cell is estimated.

The axial range resolution distance is considered first. The relation between spectral window width, f_w, and corresponding axial extent of the range cell in the medium is[14]

$$\Delta D_{\mathrm{FM}}=\frac{c}{2}\frac{f_w}{S_0}, \tag{17}$$

which is analogous to the axial range resolution distance, $\Delta D_{\mathrm{PW}}=(c/2)T_w$, for the PW–tsm Doppler system.

Before continuing with the cross-correlation function, some observations concerning (14) must be made. It is seen from (15) and (10) that consecutive magnitude fsm spectra are displaced by an amount

$$\Delta f_a=f_a^{(n+1)}-f_a^{(n)}=\frac{2\nu T_r}{c}S_0=\tau_0 S_0. \tag{18}$$

The spectral shift, Δf_a, is equal to the time shift between consecutive received PW signals *multiplied* with the time to frequency conversion factor, S_0. Specifically, it is seen that

$$|\widetilde{G}_a^{(n+1)}(f)|=|\widetilde{G}_a^{(n)}(f-\Delta f_a)|, \tag{19}$$

while

$$\widetilde{G}_a^{(n+1)}(f)\neq\widetilde{G}_a^{(n)}(f-\Delta f_a). \tag{20}$$

The latter inequality is due to the fact that the time signals from which $\widetilde{G}_a^{(n)}(f)$ and $\widetilde{G}_a^{(n+1)}(f)$ are generated are shifted both in frequency *and in time* causing the phase of $\widetilde{G}_a^{(n)}(f)$ to be shifted relatively to the phase of $\widetilde{G}_a^{(n+1)}(f)$. This can be observed by comparing plot (d) with plot (e) in Fig. 3. Also, note that the rate of oscillation of the real parts is changed by only a small amount (the relative increase is $(4\nu/c)T_r/t_m$). This means that the unique waveform signature present in received PW signals at a given range is not preserved in the real or imaginary part of $\widetilde{G}_a^{(n)}(f)$. However, as will be shown, this does not remove the possibility for velocity detection from the real part of the cross-correlation function. Whereas the result of the cross-correlation of magnitude spectra[14] can be interpreted directly by using (18), the result of cross-correlating real spectra is influenced by additional factors; nonetheless, peak detection based on the more rapidly oscillating real spectra is likely to be more precise.

The cross-correlation function for one scatterer will now be considered. In this case, the range-gate window can be ignored which makes it possible to write the complex cross-correlation function of two consecutive fsm spectra in (14) as follows:

$$\widetilde{C}_{\mathrm{FM}}^{(n,n+1)}(\gamma)=\int_{-\infty}^{\infty}\widetilde{G}_a^{(n)}(f)\widetilde{G}_a^{(n+1)*}(f+\gamma)df, \tag{21}$$

where $*$ denotes complex conjugation. Inserting (14) for n and $n+1$ into (21) allows an analytical solution to (21) to be derived. In Appendix B, this complex-valued cross-correlation function has been found to be

$$\widetilde{C}_{\mathrm{FM}}^{(n,n+1)}(\gamma)=A_C\exp\left[-\frac{\pi^2}{2\alpha_G}(\Delta f_a-\gamma)^2\right]\times\exp[-j\pi t_a^{(n)}(\Delta f_a-\gamma)+j\varphi_C^{(n)}], \tag{22}$$

where $A_C\cong r^2\sqrt{\pi/2\alpha_G}$ and

$$\varphi_C^{(n)}=\pi\tau_0[S_0(2t_d^{(n)}+\tau_0)-2f_1]. \tag{23}$$

The factor $t_a^{(n)}$ in (22) determines the ''rate of oscillation'' of the cross-correlation function where $t_a^{(n)}/2$ is in cycles per hertz:

$$t_a^{(n)}=t^{(n)}+t^{(n+1)}-2t_s+t_m=2t_d^{(n)}+\tau_0+t_m. \tag{24}$$

The result in (22) is a complex sinusoid with a Gaussian envelope. The real part of (22) is

$$C_{\mathrm{FM}}^{(n,n+1)}(\gamma)=\mathrm{Re}\{\widetilde{C}_{\mathrm{FM}}^{(n,n+1)}(\gamma)\}=A_C\exp\left[-\frac{\pi^2}{2\alpha_G}(\Delta f_a-\gamma)^2\right]\times\cos[-\pi t_a^{(n)}(\Delta f_a-\gamma)+\varphi_C^{(n)}], \tag{25}$$

which is identical to the cross-correlation of the real part of consecutive fsm spectra. A good approximation to the global maximum of the cross-correlation function in (25) has been derived in Appendix C for the case when the velocity is below the aliasing velocity, $\nu_{\mathrm{alias}}=c/(4f_0T_r)$; this maximum is given as

$$\gamma_0\cong\frac{2T_r}{c}\left(S_0+\frac{2f_1}{t_m}\right)\nu=\frac{2T_r}{c}\left(S_0+\frac{2(f_0-\frac{1}{2}B_0)}{t_m}\right)\nu=\frac{4T_r}{c}\frac{f_0}{t_m}\nu. \tag{26}$$

An estimate of γ_0, based on actual data, is found as

$$\hat{\gamma}=\underset{\gamma}{\mathrm{argmax}}\{\hat{C}_{\mathrm{FM}}^{(n,n+1)}(\gamma)\}. \tag{27}$$

Using (26) and (27), the estimate of the particle velocity is

$$\hat{\nu}=\frac{\hat{\gamma}}{(4T_r/c)(f_0/t_m)}=\frac{c\sqrt{8}\alpha t_{m,\mathrm{rms}}}{4T_rf_0}\hat{\gamma}, \tag{28}$$

where the relation between t_m and rms duration of t_m, i.e., $t_m=\sqrt{8}\alpha t_{m,\mathrm{rms}}$,[18] has been used. A numeric example of two consecutive fsm spectra is provided in Fig. 4, together with the cross-correlation function between them. Both the magnitude cross-correlation function and the complex-valued cross-correlation function are shown. The locations of their respective peaks are indicated.

The spectra in Fig. 4 were generated with the following system parameters: $f_0=3.5$ MHz, $B_0=5$ MHz, $T_r=133.3$ μs, $t_m=0.8T_r=106.7$ μs, and $S_0=46.87$ GHz/s, $\nu_{\mathrm{alias}}=c/(4f_0T_r)=0.8$ m/s. The velocity of the scatterer was $\nu=0.7\nu_{\mathrm{alias}}=0.56$ m/s. The peak of the magnitude function is at $2\nu T_r/cS_0=4.68$ kHz, while the peak of the real function is at $2\nu T_r/c(S_0+2f_1/t_m)=6.56$ kHz.

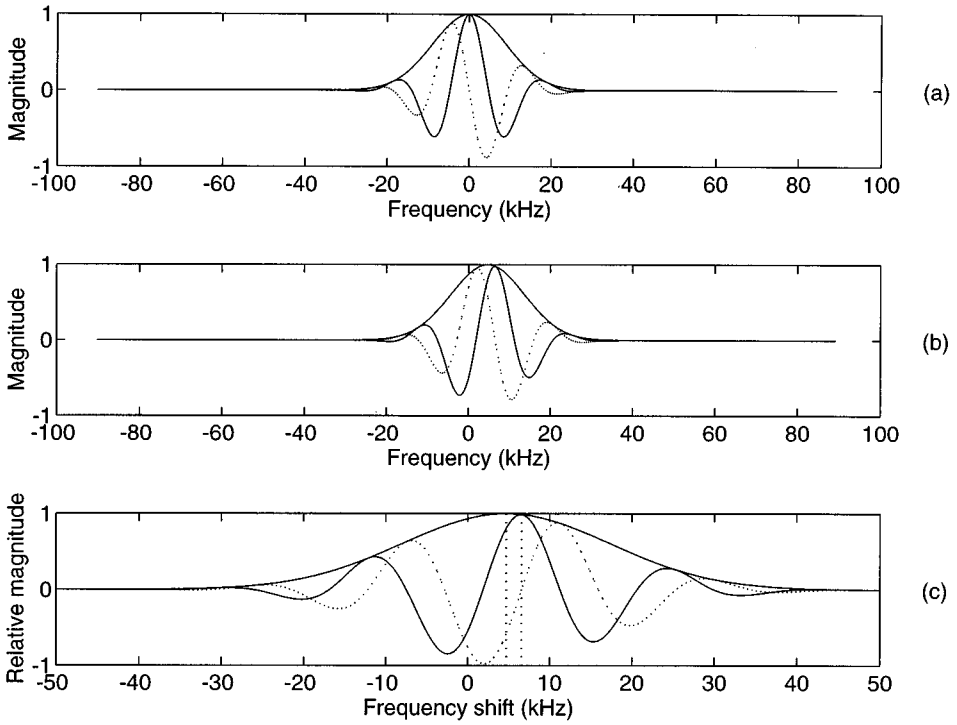

FIG. 4. Two consecutive fsm spectra and their cross-correlation function in the FM–fsm Doppler system. (a) and (b) Real part (———), imaginary part (···) and magnitude (———) of first and second fsm spectra, $\tilde{G}_a^{(n)}(f)$ and $\tilde{G}_a^{(n+1)}(f)$, respectively. Note that the real part of $\tilde{G}_a^{(n+1)}(f)$ is both shifted in frequency and modified in form, relative to the real part of $\tilde{G}_a^{(n)}(f)$. (c) Real part, imaginary part and magnitude of cross-correlation function, $\tilde{C}_{\mathrm{FM}}^{(n,n+1)}(\gamma)$, between the complex waveforms in (a) and (b). The *magnitude* corresponds to the result of cross-correlating the magnitude spectra in (a) and (b). The peak is located at $(2\nu T_r/c)S_0=4.68$ kHz and indicated in (c) with a vertical dotted line. The *real part* corresponds to the result of cross-correlating the real parts of (a) and (b). The peak is here located at $(2\nu T_r/c)(S_0+2f_1/t_m)=6.56$ kHz, also shown with a vertical dotted line.

IV. COMPARISON BETWEEN PW–tsm AND FM–fsm DOPPLER SYSTEMS

Based on the description of the two Doppler systems in Sec. III, their relative performance will now be compared. As mentioned earlier, the performance of a Doppler system is evaluated by the size of the spatial resolution cell, and by how precisely the velocity is found within this resolution cell.

It is assumed that the rms bandwidths, $B_{\mathrm{PW,rms}}$ and $B_{\mathrm{FM,rms}}$, of the transmitted PW and FM signals, respectively, are identical. Also, the mean transmitted energy and the noise signal power level at the receiving transducers are assumed identical in the two Doppler systems. The validity of these assumptions in practice is discussed at the end of this section.

The *range cell size* (spatial resolution) is determined *laterally* by the beam dimensions and *axially* by the bandwidth of the transmitted/received signal *and* the window length (defined by T_w or f_w, for PW–tsm and FM–fsm, respectively). In this paper, only the axial resolution distances are compared, as the lateral dimension is determined mainly by the transducer geometry and aperture size, i.e., transducer dimensions measured in wavelengths.

When the received signal in the PW Doppler system, $g_r^{(n)}(t)$, for *one scatterer* is compared with the fsm spectrum, $\tilde{G}_a^{(n)}(f)$, for *one scatterer*, several similarities and parallels are seen: First of all, when the scatterer is moved along the acoustic axis of the transducer, the envelope of the received PW signal, $|g_{r,\mathrm{PW}}^{(n)}(t)|$, is shifted on the time axis just as the fsm spectrum *envelope*, $|\tilde{G}_a^{(n)}(f)|$, is shifted on the frequency axis. Both these axes thus represent range in their respective Doppler systems. Second, if $\Delta D_{\mathrm{PW}}=cT_w/2=\Delta D_{\mathrm{FM}}=cf_w/(2S_0)$, it can be shown analytically that the resulting axial range resolution distance is identical for the two systems.

The performance of the peak detection of the cross-correlation function can be evaluated by comparing the input signals to the cross-correlation and the cross-correlation function itself. With the above stated assumptions, analytical analysis of the signal-to-noise ratio (SNR) reveals that the SNR for the input signals in the PW–tsm Doppler system is identical to the SNR for the input spectra in the FM–fsm Doppler system. Finally, consider the behavior of the cross-correlation functions. In addition to the aforementioned values for ΔD_{PW} and ΔD_{FM}, assume that a search window is applied to the cross-correlation functions, such that only velocities in the range of $\pm\nu_{\mathrm{alias}}$ can be detected. It can then be shown analytically that the cross-correlation functions with high probability will contain exactly one cycle within the search window, even though the real input waveforms to the cross-correlator behave differently for the PW–tsm and the FM–fsm Doppler systems. Thus there is very little risk of detecting a sidelobe in the cross-correlation function. The results show that performance of the two Doppler systems should be roughly the same.

In a practical implementation, the operating conditions

of the PW and FM Doppler systems may differ in several aspects. Due to the relationship between bandwidth and peak power in pulsed systems (assuming constant mean power), PW Doppler systems may not be able to utilize the full bandwidth afforded by the transducer whereas the bandwidth limitation of the FM Doppler system can be assumed to be that of the transducer; these factors may give the FM Doppler system a better axial resolution and improve the velocity estimate. In the measurement situations where a peak power limitation is encountered (e.g., due to cavitation and/or nonlinearities) before a mean power limitation, the FM Doppler system can operate at a higher mean power level, thus giving an improved SNR relative to the PW Doppler system.

V. SIMULATION COMPARISONS

In order to provide a limited evaluation of the performance of the two Doppler systems, a few simulation results are presented.

A 2-D flow situation, simulating parabolic flow in a rigid tube, was modeled. The received signals were calculated from a large number of scattering particles, according to (11), randomly distributed inside the region from where backscattered signals would be received. The model[13] includes both *lateral variation in ultrasound beam intensity* and *velocity variation within the range cell*. The scattering coefficient was chosen to be frequency independent.

The parameters common to both systems were as follows: $f_0=5$ MHz, $B_{\text{rms}}=1.06$ MHz, $\alpha=3$; $D_{\max}=0.075$ m; $T_r=2D_{\max}/c=100$ μs; $\nu_{\text{alias}}=0.75$ m/s. The maximal flow velocity in direction of the beam was: $\nu_{\max}=0.85\nu_{\text{alias}}=0.64$ m/s. $L=2$ and SNR=20 dB. The shapes of the mean spectrum of the signal and the mean spectrum of the noise were identical (Gaussian). The parameters for the PW Doppler system were: $t_{m,\text{PW}}=637$ ns$=3.2/f_0$ [obtained from $B_{\text{rms}}=\alpha/(\sqrt{2}\pi/t_{m,\text{PW}})$]. $T_w=8/f_0$, giving $\Delta D=cT_w/2=1.2$ mm. The specific parameters for the FM Doppler system were: $B_0=9$ MHz [obtained from $B_{\text{rms}}=B_0/(\sqrt{8}\alpha)$] which yields $f_1=0.5$ MHz and $f_2=9.5$ MHz; $t_{m,\text{FM}}=0.8T_r=80$ μs.

The result of 3000 independent repetitions of the simulations is given in Fig. 5(a) and (b) which shows the mean velocity profiles together with ± 1 s.d. for the PW and FM Doppler systems, respectively. It was verified that doubling the number of repetitions and doubling the scatterer density did not change the results noticeably. As seen from these results, the two systems function nearly identically. The slightly better performance of the PW-tsm Doppler system may be due to sidelobes in the fsm spectrum.

VI. EXPERIMENTAL COMPARISON

This section presents the experimental system and the measured velocity profiles for the PW and FM Doppler systems. Note that the experimental results to be presented are included to give a mainly qualitative experimental proof of concept and should not be seen primarily as a verification of the analytical results.

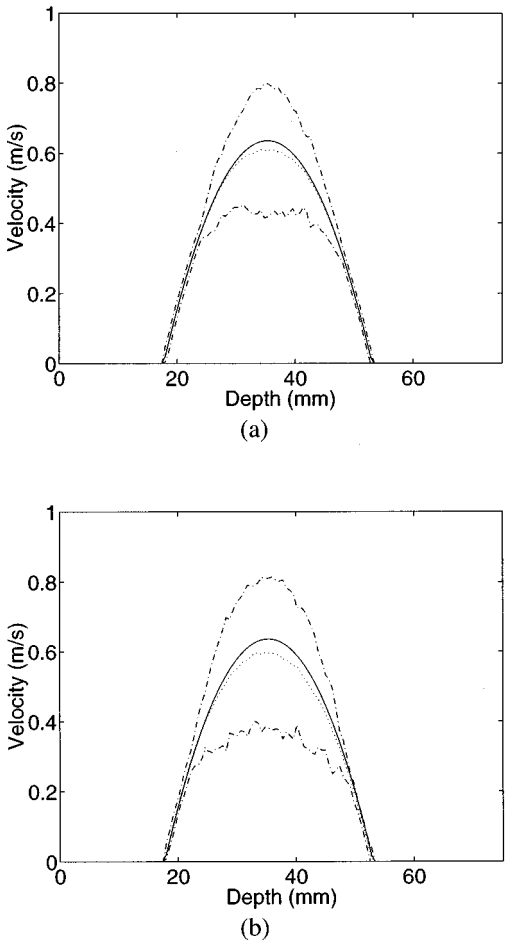

FIG. 5. Mean velocity profiles (·····) shown with ± one standard deviation (-·-·-) obtained with simulation model. The true velocity profile, TVP (—), (known *a priori*) is shown together with the velocity profiles obtained with the PW–tsm Doppler system in (a) and the FM–fsm Doppler system in (b). The results are obtained from 3000 independent profiles, each estimated with a signal-to-noise ratio of 20 dB. See text for additional parameters.

A. Description of experimental setup

An experimental Doppler system has been developed for the purpose of making both FM–fsm and PW–tsm Doppler measurements. The measurement system is shown in Fig. 6 and consists of: (1) a DOS-based computer; (2) an *arbitrary function generator* (AFG), *LeCroy* 9100, generating the transmitted signal in analog form; (3) a *power amplifier* (PA), *Amplifier Research* 50A15, driving the transmitting transducer; (4) a *focused dual element annular array ultrasonic transducer* (*Echo Ultrasound*), for simultaneous transmission and reception of ultrasound; and (5) a *digital storage oscilloscope* (DSO), *LeCroy* 9400, with which the received signal was digitized and transferred to the computer.

Discrete representations of the transmission signals (sweep signals for the FM and burst signals for the PW Doppler, respectively) were generated in the computer and loaded onto the AFG with a sampling frequency of 25 MHz. The signal from the AFG was subsequently amplified to an appropriate level for the transducer. The transducer had a nominal center frequency of 3.75 MHz, a diameter of 14.7 mm and produced an extended focal region between 32 and 65 mm. In all the experiments, the annular array uses one

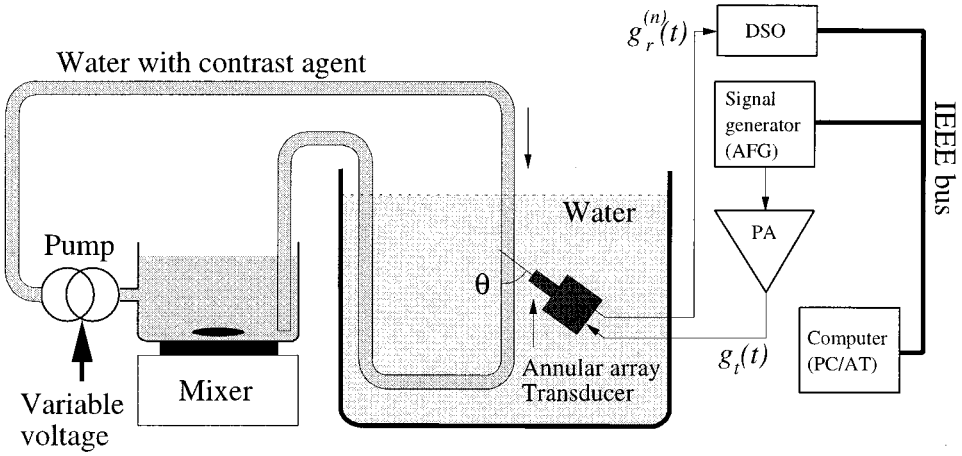

FIG. 6. The experimental system. A centrifugal pump is circulating a mixture of water and corn starch. The pump is controlled by a variable voltage to achieve different flow rates. The transmission signal is generated by the arbitrary function generator (AFG) which sends the signal to the power amplifier (PA). The transmitting part of the transducer is connected to the power amplifier, while the receiving part is connected to the digital storage oscilloscope (DSO). Both the AFG and the DSO are controlled from a personal computer via a GPIB (IEEE-488) bus.

ring for transmission and one ring for reception. By means of the DSO, 32 000 eight-bit samples of the received signal were subsequently recorded and stored. The sampling frequency was set of 12.5 MHz, limiting the total observation time, T_{obs}, to 2.56 ms. The signal processing scheme was done exclusively in the computer. A stationary echo canceler (SEC) was included to remove stationary echoes.

The flow phantom is also shown in Fig. 6. A centrifugal pump circulated a mixture of water and corn starch (2%–5% vol.) from a reservoir. The water in the reservoir was stirred with a magnetically driven stirring device in order to avoid aggregation of the corn starch. The pump was controlled by a variable voltage to obtain different flow rates. The tube segment, where the measurements were taken, consisted of heat shrinking tubes of various diameters, suspended inside a water-filled scanning tank. The tube diameters were selected in such a way that they correspond to larger human arteries. The tube was suspended vertically to achieve a symmetric velocity profile and the flow was measured in the lower end of this tube.

The systems parameters common for the two systems are: $T_r=80$ μs, $D_{\max}=60$ mm, $L=32$ (number of transmitted signals), and $c=1500$ m/s. The parameters for the transmitted signal for the PW–tsm Doppler system were as follows: $f_0=3.5$ MHz, $t_m=4/f_0$, $\nu_{\text{alias}}=c/(4f_0T_r)=1.33$ m/s. The parameters for the transmitted signal for the FM–fsm Doppler system were: $f_1=2.75$ MHz, $f_2=4.75$ MHz, $f_0=3.75$ MHz, $t_m=60$ μs, and $\nu_{\text{alias}}=c/(4f_0T_r)=1.25$ m/s. In both systems, a rectangular envelope was used for the transmitted signals sent from the AFG to the ultrasound transducer. The range cell size was $\Delta D_{\text{PW}}=\Delta D_{\text{FM}}=2$ mm for a total of 29 range cells. Both larger and smaller resolution cells were tried in the signal processing, but without obtaining more precise velocity estimates. Specifically, increasing the axial resolution distance (increasing T_w) yielded a poorer cross-correlation function estimate as the range cell in this case contained a larger velocity variation. On the other hand, lowering T_w gave shorter input signals to the cross-correlation function, which also degraded the estimate. The ''true'' peak in the discrete cross-correlation function was estimated from a three-point parabolic fit[8] around the peak value in the discrete cross-correlation function.

B. Performance of measurement system

In Sec. IV, the two Doppler systems were compared and the performances were found to be roughly identical, assuming the same bandwidth of the transmitted signal and the same signal-to-noise ratio.

In the experimental system, the bandwidth of the transmitted signals was evaluated and found to be slightly larger for the FM Doppler system than for the PW Doppler system. Furthermore, the spectra of the transmitted FM signals deviated significantly from a Gaussian shape. Consequently, the compensation/conversion parameter used in (28) is not valid. A correction factor was empirically found to be 1.4, such that the velocity estimates found from (28) had to be multiplied with 1.4 to yield the correct result.

The signal-to-noise ratio depends on several factors: The level of energy transmitted, the background noise level, and the dynamic range of the digitizing equipment. The background noise level was identical in the two Doppler system. The transmitted energy, however, was much higher for the FM Doppler system than for the PW Doppler system. However, as the background noise level was quite low, this advantage in transmitted power did not carry any performance improvement for the FM Doppler system over the PW Doppler system. Furthermore, the FM Doppler system had a serious drawback due to significant electric cross-talk in the transducer which combined with the received signals from the flow region. As a result, the output of the digital stationary echo canceler (SEC) was represented by only a few bits, specifically, 7 bits for the PW Doppler system versus only 3 bits for the FM Doppler system. The corresponding signal-to-noise ratios[20] were approximately 44 and 20 dB, respectively. These findings are consistent with the results in Table

TABLE I. Flow values for the experimental results. Angle between flow direction and ultrasound beam, θ=60°. Tube diameter, d_ν=2 cm and corresponding cross-sectional area A_ν=3.14 cm^2. $\overline{\nu}$ and $\overline{\nu_b}$ are the particle velocities in the direction of the tube and in the direction of the ultrasound beam, respectively. $\overline{\rho_{\text{meas}}}$ is average of the cross-correlation coefficient over the tube. The density of the fluid was 1000 kg/m^3 and the dynamic viscosity was 0.001 Ns/m^2.

Figure	$\dot{Q}$ (m^3/s)	$\overline{\nu}$ (m/s)	$\overline{\nu_b}$ (m/s)	R_e ⋯	PW $\overline{\rho_{\text{meas}}}$	FM $\overline{\rho_{\text{meas}}}$
7(a)	9.3×10^{-5}	0.3	0.15	6000	0.95	0.73
7(b)	2.2×10^{-4}	0.7	0.35	14 000	0.96	0.80
7(c)	3.16×10^{-4}	1.0	0.5	20 000	0.97	0.85

I which shows the cross-correlation coefficient, ρ_{meas}, in the actual situation. The level of $\overline{\rho_{\text{meas}}}$ is much lower for the FM case. Note that the cross-correlation coefficients at the peak value of the cross-correlation function, ρ_{nf}, in the absence of cross talk and noise, are roughly identical in the two Doppler systems, as the measurement situations (including PW and FM beam shapes) were roughly the same.

C. Velocity profiles

Since measurements on phantoms can never be accurately simulated, one fundamental problem arises: There is no reference velocity profile to which the experimental results can be compared. In order to be able to estimate the shape of the velocity profiles, the phantom was optimized mechanically to minimize flow perturbation. The velocities were chosen to represent typical velocities in the major arteries; this resulted in Reynolds numbers greater than or equal to 6000 for all the flow velocities in the experiments. It is here assumed, and supported by simple viscosity measurements, that the corn starch only produces minimal change in viscosity. Whereas Reynolds numbers in the region from roughly 2500 to 6000 (the upper limit is dependent on the tube smoothness and other experimental parameters) produce the so-called transition region flow which is chaotic and whose profile is not readily predictable,[21] flow at higher Reynolds numbers is characterized by a mean velocity profile which is approximately flat, although the corresponding instantaneous velocity profile exhibits significant random local fluctuations. The experimental results represent a mean velocity profile, as they are based on the average of 32 sweeps, corresponding to a time average over 2.56 ms.

In Fig. 7(a)–(c), velocity profiles are presented for the three different flow velocities listed in Table I. The velocity profiles are power-gated, i.e., when the power, after stationary echo canceling, in a given range cell falls below a pre-set threshold value, the detected velocity is set to zero for that range cell. The flow measurements were all carried out with the use of a simple stationary echo canceler. To investigate possible differences in behavior for PW and FM signals, we have modeled the transfer function of the stationary echo canceler as a function of flow velocity and bandwidth of the excitation signal, for both the PW and FM Doppler signals. The results showed that the transfer functions are very similar, albeit not identical, when realistic bandwidths are used.

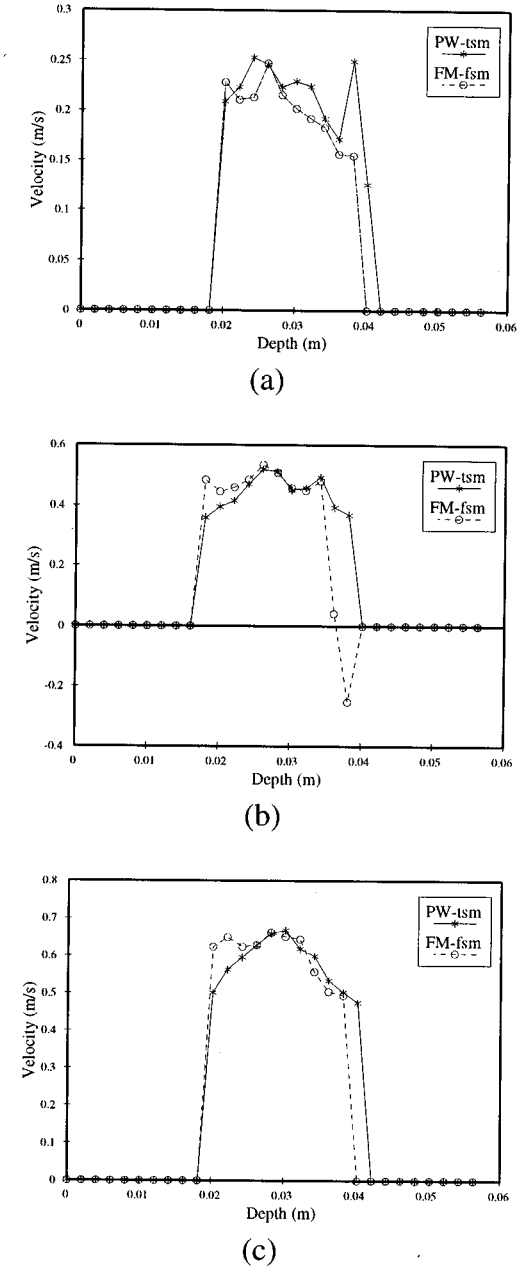

FIG. 7. Measured velocity profiles for PW-tsm and FM-fsm Doppler systems. See Table I for parameter values.

All the measured velocity profiles exhibit a reasonably good agreement with the directly measured volume flows. As the Reynolds numbers in all cases far exceed the limit for laminar flow, the mean velocity profiles are approximately flat, except near the tube walls, and with rapid local fluctuations, as has also been demonstrated with laser Doppler velocimetry and with bubble visualization.[21] With respect to the width of the flow profiles, relative large variations could be seen near the location of the back wall which possibly may be due to attenuation by very small air bubbles across the tube. This variation makes it more difficult to verify the mean velocity.

VII. DISCUSSION AND CONCLUSIONS

In this paper, a velocity profiling system based on the transmission of coherent repetitive frequency-modulated

sweep signal has been analyzed analytically, compared to the PW Doppler system utilizing time-shift measurements, and evaluated with simulations and experiments. A specific advantage of the FM Doppler system is the much lower peak power relative to the conventional PW Doppler systems. This FM–fsm Doppler system is based on cross-correlation of the real parts of consecutive so-called fsm spectra, analogous to the cross-correlation of consecutive received signal segments in a PW–tsm Doppler system. The flow velocity is estimated from the peak location in this cross-correlation function. As the peak can occur anywhere in the function, the PW–tsm and FM–fsm Doppler systems do not suffer from the aliasing phenomena, known from Doppler systems using phase shift measurement. On the other hand, under poor SNR conditions these new systems risk detecting one of the sidelobes in the cross-correlation function as the peak, thus providing an erroneous result. This problem may be circumvented by only searching for the peak in the region that corresponds exactly to the aliasing-free velocity range in a psm Doppler system. However, in this case, the cross-correlation-based Doppler systems function in the same way as the psm Doppler systems.

The factors determining the performance of the two systems were found to be very similar, arguing for a similar performance of the two systems. This is supported by the preliminary simulation results which show that under matched conditions (bandwidth and SNR), the two systems perform very similarly.

The feasibility of measuring flow profiles with the FM and PW Doppler systems on a simple flow model under semirealistic conditions has been demonstrated. In order to validate the applicability in the area of medical diagnostic ultrasound, experiments with a soft tissue-like coupling medium and *in vivo* experiments must be carried out.

Considering that the experimental system suffered from severe cross-talk for the FM–fsm measurements and therefore had insufficient dynamic range, combined with the fact that the shape of the transmitted signal envelope was very different from a Gaussian shape, the profiles obtained with the PW and FM Doppler systems nevertheless agree quite well. The PW–tsm and FM–fsm profiles appear reasonable and the reproducibility was quite good. This indicates that the flow phantom and the measurement system, as such, functioned properly.

ACKNOWLEDGMENTS

The authors would very much like to thank Jean-Marie Bordier for valuable discussions. The authors would also like to thank Uno Junghans and Jørn Lund, Brüel & Kjær A/S, for help with respect to computer solutions. This work was partly supported by the National Science Foundation under grant BCS-9009886 and by the following Danish foundations: The Research Academy, Thomas B. Thrige's Foundation, V. S. Trane's Foundation, and H. C. Ørsteds Foundation.

APPENDIX A: DERIVATION OF $\tilde{G}_a^{(n)}(f)$

In this Appendix, the demodulated signal, $\tilde{g}_a^{(n)}(t)$, and its spectrum, $\tilde{G}_a^{(n)}(f)$, are derived. From (13) we have for a single scatterer that

$$\begin{aligned}\tilde{g}_a^{(n)}(t) &= 2\mathrm{LP}\{g_r^{(n)}(t)\tilde{g}_{\mathrm{ref}}(t)\}\\ &\cong r\ \exp\left[-\alpha_G\left(t-t^{(n)}-\frac{t_m}{2}\right)^2\right]\\ &\quad\times 2\mathrm{LP}\{\mathrm{Re}\{\exp[j(2\pi f_1(t-t^{(n)})\\ &\quad+\pi S_0(t-t^{(n)})^2)]\}\\ &\quad\times\exp[j(2\pi f_1(t-t_s)+\pi S_0(t-t_s)^2)]\},\\ &\quad t^{(n)}\leqslant t\leqslant t^{(n)}+t_m\end{aligned}\tag{A1}$$

Setting

$$\begin{aligned}\theta_r &= 2\pi f_1(t-t^{(n)})+\pi S_0(t-t^{(n)})^2,\\ \theta_{\mathrm{ref}} &= 2\pi f_1(t-t_s)+\pi S_0(t-t_s)^2\end{aligned}\tag{A2}$$

we can write the terms being processed by the ideal low-pass filter as

$$\begin{aligned}&2\mathrm{LP}\{e^{j\theta_{\mathrm{ref}}}\,\mathrm{Re}\{e^{j\theta_r}\}\}\\ &\quad=2\mathrm{LP}\{e^{j\theta_{\mathrm{ref}}}\cos(\theta_r)\}\\ &\quad=2\mathrm{LP}\left\{\frac{\exp[j(\theta_{\mathrm{ref}}+\theta_r)]+\exp[j(\theta_{\mathrm{ref}}-\theta_r)]}{2}\right\}\\ &\quad=\exp[j(\theta_{\mathrm{ref}}-\theta_r)],\end{aligned}\tag{A3}$$

so that

$$\begin{aligned}\tilde{g}_a^{(n)}(t) &= r\ \exp\left\{-\alpha_G\left[t^2+\left(t^{(n)}+\frac{t_m}{2}\right)^2-2\left(t^{(n)}+\frac{t_m}{2}\right)t\right]\right\}\\ &\quad\times\exp[j\pi[2f_1(t^{(n)}-t_s)+S_0(t_s^2-(t^{(n)})^2)\\ &\quad+2S_0(t^{(n)}-t_s)t]],\quad t^{(n)}\leqslant t\leqslant t^{(n)}+t_m.\end{aligned}\tag{A4}$$

To simplify the notation of (A4), the following terms will be defined:

$$\begin{aligned}t_d^{(n)} &\equiv t^{(n)}-t_s,\\ a_{\mathrm{env}}^{(n)}(t) &\equiv \exp\left[-\alpha_G t^2+2\alpha_G\left(t^{(n)}+\frac{t_m}{2}\right)t\right],\\ A_0^{(n)} &\equiv r\ \exp\left[-\alpha_G\left(t^{(n)}+\frac{t_m}{2}\right)^2\right],\\ \varphi_a^{(n)} &\equiv \pi[2f_1t_d^{(n)}+S_0(t_s^2-(t^{(n)})^2)].\end{aligned}\tag{A5}$$

In (A5), $A_0^{(n)}$ is a constant amplitude term, $a_{\mathrm{env}}^{(n)}(t)$ represents the envelope function of $\tilde{g}_a^{(n)}(t)$, and $\varphi_a^{(n)}$ describes a constant phase term. By means of these terms, (A4) can be expressed as follows:

$$\tilde{g}_a^{(n)}(t)=A_0^{(n)}a_{\mathrm{env}}^{(n)}(t)\exp[j(2\pi S_0t_d^{(n)})t+j\varphi_a^{(n)}].\tag{A6}$$

As $\tilde{g}_a^{(n)}(t)$ only physically exists for $t\geqslant t_s$ due to the t_s seconds delay of the demodulating sweep signal, it is appropriate to use $t=t_s$ as the zero time reference when calculat-

ing $\tilde{G}_a^{(n)}(f)$. In other words, the spectrum of $\tilde{g}_a^{(n)}(t+t_s)$ is to be found where

$$\tilde{g}_a^{(n)}(t+t_s)=A_0^{(n)}a_{\text{env}}^{(n)}(t+t_s)\exp[j2\pi S_0 t_d^{(n)}(t+t_s) + j\varphi_a^{(n)}]. \tag{A7}$$

Before doing that, (A7) will be simplified further. Through straightforward arithmetic manipulation, it can be shown that

$$A_0^{(n)}a_{\text{env}}^{(n)}(t+t_s)=r\ \exp\left[-\alpha_G\left(t_d^{(n)}+\frac{t_m}{2}\right)^2\right] \times\exp\left[-\alpha_G t^2+2\alpha_G\left(t_d^{(n)}+\frac{t_m}{2}\right)t\right]. \tag{A8}$$

By defining the following two new terms:

$$B_0^{(n)}\equiv r\ \exp\left[-\alpha_G\left(t_d^{(n)}+\frac{t_m}{2}\right)^2\right] \tag{A9}$$

and

$$\varphi_b^{(n)}=\pi t_d^{(n)}(2f_1-S_0t_d^{(n)}),$$

the complex spectrum of this signal, $\tilde{G}_a^{(n)}(f)$, can be found as

$$\begin{aligned}\tilde{G}_a^{(n)}(f)&=\int_{-\infty}^{\infty}\tilde{g}_a^{(n)}(t+t_s)e^{-j2\pi ft}\,dt\\ &=B_0^{(n)}\ \exp[j\varphi_b^{(n)}]\int_{-\infty}^{\infty}\exp\left\{-\alpha_G t^2 -\left[-2\alpha_G\left(t_d^{(n)}+\frac{t_m}{2}\right)-j2\pi(S_0t_d^{(n)}-f)\right]t\right\}dt.\end{aligned} \tag{A10}$$

A closed form solution to (A10) can be obtained from the following integral solution:[22]

$$\int_{-\infty}^{\infty}\exp(-\beta^2x^2-\gamma x)dx=\frac{\sqrt{\pi}}{\beta}\exp\left(\frac{\gamma^2}{4\beta^2}\right),\quad \text{Re}(\beta)>0. \tag{A11}$$

Using (A11), (A10) can be written in analytical form as

$$\tilde{G}_a^{(n)}(f)=B_0^{(n)}\sqrt{\frac{\pi}{\alpha_G}}\exp[j\varphi_b^{(n)}] \times\exp\left[\frac{[-2\alpha_G(t_d^{(n)}+t_m/2)-j2\pi(S_0t_d^{(n)}-f)]^2}{4\alpha_G}\right]. \tag{A12}$$

Collecting terms and introducing

$$f_a^{(n)}=t_d^{(n)}S_0=(t^{(n)}-t_s)S_0=\frac{2(d^{(n)}-D)}{c}S_0, \tag{A13}$$

which is the center frequency of the spectrum (or the so-called *position frequency*[15] of the fsm spectrum) makes it possible to write (A12) as

$$\tilde{G}_a^{(n)}(f)=\sqrt{\frac{\pi}{\alpha_G}}\,B_0^{(n)}\ \exp[j\varphi_b^{(n)}]\exp\left[\alpha_G\left(t_d^{(n)}+\frac{t_m}{2}\right)^2\right] \times\exp\left\{-\frac{\pi^2}{\alpha_G}(f_a^{(n)}-f)^2+j\left[2\pi\left(t_d^{(n)}+\frac{t_m}{2}\right) \times(f_a^{(n)}-f)\right]\right\}. \tag{A14}$$

It is readily seen from (A9) that $B_0^{(n)}\exp[\alpha_G(t_d^{(n)}+t_m/2)^2]$ evaluates to the reflection coefficient, r. We can thus finally write (A14) as

$$\tilde{G}_a^{(n)}(f)=r\sqrt{\frac{\pi}{\alpha_G}}\exp\left[-\frac{\pi^2}{\alpha_G}(f_a^{(n)}-f)^2\right] \times\exp\left[j2\pi\left(t_d^{(n)}+\frac{t_m}{2}\right)(f_a^{(n)}-f)+j\varphi_b^{(n)}\right]. \tag{A15}$$

APPENDIX B: DERIVATION OF THE COMPLEX CORRELATION FUNCTION $\tilde{C}_{\text{FM}}^{(n,n+1)}(\gamma)$

The formulation of the cross-correlation function is given in (21) as follows:

$$\tilde{C}_{\text{FM}}^{(n,n+1)}(\gamma)=\int_{-\infty}^{\infty}\tilde{G}_a^{(n)}(f)\tilde{G}_a^{(n+1)*}(f+\gamma)df. \tag{B1}$$

Inserting the result from (A15) gives

$$\begin{aligned}\tilde{C}_{\text{FM}}^{(n,n+1)}(\gamma)=r^2\int_{-\infty}^{\infty}&\sqrt{\frac{\pi}{\alpha_G}}\exp\left[-\frac{\pi^2}{\alpha_G}(f_a^{(n)}-f)^2\right] \times\exp\left[j2\pi\left(t_d^{(n)}+\frac{t_m}{2}\right)(f_a^{(n)}-f)+j\varphi_b^{(n)}\right]\\ &\times\sqrt{\frac{\pi}{\alpha_G}}\exp\left[-\frac{\pi^2}{\alpha_G}(f_a^{(n+1)}-f-\gamma)^2\right]\\ &\times\exp\left[-j2\pi\left(t_d^{(n)}+\tau_0+\frac{t_m}{2}\right)\right.\\ &\left.\times(f_a^{(n+1)}-f-\gamma)-j\varphi_b^{(n+1)}\right]df,\end{aligned} \tag{B2}$$

where $\tau_0=t^{(n+1)}-t^{(n)}=(2\nu T_r)/c$ is introduced, giving $t^{(n+1)}-t_s=t_d^{(n)}+\tau_0$. Here, τ_0 represents the change in round-trip travel time to the scatterer from one emitted sweep to the next.

Introducing $\Delta f_a=f_a^{(n+1)}-f_a^{(n)}=2\nu T_rS_0/c=\tau_0S_0$, as defined in (18), $\gamma'=\Delta f_a-\gamma$, and $f'=f_a^{(n)}-f$ allows (B2) to be written as

$$\begin{aligned}\tilde{C}_{\text{FM}}^{(n,n+1)}&(\Delta f_a-\gamma')\\ &=r^2\sqrt{\frac{\pi}{2\alpha_G}}\exp\left[-\frac{\alpha_G\tau_0^2}{2}\right]\exp\left[-\frac{\pi^2}{2\alpha_G}\gamma'^2\right]\\ &\quad\times\exp[-j\pi(2t_d^{(n)}+\tau_0+t_m)\gamma'+j(\varphi_b^{(n)}-\varphi_b^{(n+1)})].\end{aligned} \tag{B3}$$

Define

$$t_a^{(n)} \equiv 2t_d^{(n)} + \tau_0 + t_m = \frac{4d^{(0)} + 2\nu(2n+1)T_r}{c} - 2t_s + t_m \tag{B4}$$

and

$$A_C = r^2 \sqrt{\frac{\pi}{2\alpha_G}} \exp\left[-\frac{\alpha_G}{2} \tau_0^2 \right] \cong r^2 \sqrt{\frac{\pi}{2\alpha_G}}, \tag{B5}$$

where the last approximation is valid for all realistic velocities (i.e., $|\nu| < 5$ m/s). In addition, define

$$\varphi_C^{(n)} = \varphi_b^{(n)} - \varphi_b^{(n+1)} = \pi\tau_0[S_0(2t_d^{(n)} + \tau_0) - 2f_1]. \tag{B6}$$

Equations (B4), (B5), and (B6) make it possible to write (B3) as

$$\tilde{C}_{\mathrm{FM}}^{(n,n+1)}(\gamma) = A_C \exp\left[-\frac{\pi^2}{2\alpha_G} (\Delta f_a - \gamma)^2 \right] \times \exp[-j\pi t_a^{(n)}(\Delta f_a - \gamma) + j\varphi_C^{(n)}]. \tag{B7}$$

APPENDIX C: LOCATION OF PEAK IN $C_{\mathrm{FM}}^{(n,n+1)}(\gamma)$

In this Appendix, an expression is derived for the location of the peak in the real part of $\tilde{C}_{\mathrm{FM}}^{(n,n+1)}(\gamma)$ which is the complex cross-correlation function of consecutive fsm spectra. The real part of $\tilde{C}_{\mathrm{FM}}^{(n,n+1)}(\gamma)$ is

$$\mathrm{Re}\{\tilde{C}_{\mathrm{FM}}^{(n,n+1)}(\gamma)\} = A_C \exp\left[-\frac{\pi^2}{2\alpha_G} (\Delta f_a - \gamma)^2 \right] \times \cos[-\pi t_a^{(n)}(\Delta f_a - \gamma) + \varphi_C^{(n)}]. \tag{C1}$$

For ease of notation, the following terms are introduced:

$$f(\gamma) = \frac{1}{A_C} \mathrm{Re}\{\tilde{C}_{\mathrm{FM}}^{(n,n+1)}(\gamma)\}, \quad A = \frac{\pi^2}{2\alpha_G}, \quad B = \pi t_a^{(n)}, \quad C = \varphi_C^{(n)}, \tag{C2}$$

where $\varphi_C^{(n)}$ is given in (B6). Equation (C1) can now be written as

$$f(\gamma) = \exp[-A(\Delta f_a - \gamma)^2]\cos[-B(\Delta f_a - \gamma) + C]. \tag{C3}$$

Let γ_0 be the value of γ at which $f(\gamma)$ has a maximum, or equivalently, $\dot{f}(\gamma) = 0$. Setting $\dot{f}(\gamma_0) = 0$ yields

$$B(\Delta f_a - \gamma_0) - C = -\arctan\left[\frac{2A}{B} (\Delta f_a - \gamma_0) \right]. \tag{C4}$$

In order to solve and simplify (C4), several approximations must be made. To justify the approximations, the errors associated with the approximated expressions for the peak location will subsequently be evaluated, based on the correct peak location specified in (C1), and shown to be acceptably small.

The first approximation is a linearization of (C4). The maximum value of the argument to the arctan function is

$$\max\left(\frac{2A}{B} (\Delta f_a - \gamma_0) \right) \cong \frac{\pi t_m}{2\alpha^2} \max(\Delta f_a - \gamma_0) < \frac{\pi t_m}{2\alpha^2} \frac{S_0}{2f_0} = \frac{\pi}{4\alpha^2} \cong 0.09. \tag{C5}$$

The following approach is used in evaluating (C5): $\max(\Delta f_a - \gamma_0) < \max(\Delta f_a) = (2T_r S_0/c)\nu_{\mathrm{alias}} = (S_0/2 f_0)$, where the term $\max(\Delta f_a - \gamma_0)$ represents the maximum difference between the peak locations in the magnitude and real part of the cross-correlation function. In addition, $B_0 = f_0$ and $\alpha = 3$. From (C5) it is seen that the upper bound of the argument is sufficiently small for (C4) to be linearized. This means that (C4) can be approximated to

$$B(\Delta f_a - \gamma_0) - C \cong -\frac{2A}{B} (\Delta f_a - \gamma_0) \tag{C6}$$

giving

$$\gamma_0 \cong \Delta f_a - \frac{BC}{2A + B^2}, \tag{C7}$$

Δf_a is the spectral shift observed in the magnitude spectra, thus the term "$BC/(2A+B^2)$" gives the correction to this spectral shift. By using that $t_a^{(n)} = 2t_d^{(n)} + \tau_0 + t_m \cong 2t_d^{(n)} + t_m$, (as $2\nu \ll c$ and $t_m \cong T_r$) and that $S_0\tau_0 - 2f_1 = (\tau_0/t_m)B_0 - 2f_1 \cong -2f_1$ (as $\tau_0/t_m << 1$), the following simplification can be made:

$$\frac{BC}{2A + B^2} = \frac{\pi t_a^{(n)} \varphi_C^{(n)}}{\pi^2/\alpha_G + (\pi t_a^{(n)})^2} \cong \frac{(2t_d^{(n)} + t_m)\tau_0(2S_0 t_d^{(n)} - 2f_1)}{(2t_d^{(n)} + t_m)^2 + 1/\alpha_G}. \tag{C8}$$

By further assuming that

$$\frac{B_0}{f_1} \frac{|t_d^{(n)}|}{t_m} \ll 1; \quad 2\frac{|t_d^{(n)}|}{t_m} \ll 1; \quad \frac{1}{2\alpha^2} \ll 1, \tag{C9}$$

(C8) can finally be simplified to

$$\frac{BC}{2A + B^2} \cong -\frac{2f_1}{t_m} \frac{2\nu}{c} T_r. \tag{C10}$$

By use of (C10), (C7) can be written as

$$\gamma_0 \cong \frac{2\nu T_r}{c} \left(S_0 + \frac{2f_1}{t_m} \right). \tag{C11}$$

Eventually, the velocity can be found from (C11) as

$$\hat{\nu} \cong \frac{\gamma_0}{(2T_r/c)(S_0 + 2f_1/t_m)}. \tag{C12}$$

In order to quantify the error committed with the two levels of approximations, a simulation program was used to find the correct peak from (C1) and compare this with the two results in (C7) and (C11). Using the following parameters: $\alpha = 3$; $c = 1500$ m/s; $D_{\max} = 0.1$ m; $T_r = 2D_{\max}/c = 113$ μs; $D = D_{\max}/2$; $d = D$; $f_0 = 3.5$ MHz; $B_0 = 5$ MHz; $t_m = 0.8T_r$, resulted in a relative error that was less than 0.1% and 1.65% for (C7) and (C11), respectively, when evaluated over $[-\nu_{\mathrm{alias}}; \nu_{\mathrm{alias}}]$. These figures are much smaller

than errors normally associated with ultrasonic blood flow measurement.

[1] P. Atkinson and J. P. Woodcock, *Doppler Ultrasound and its Use in Clinical Measurements* (Academic, London, UK, 1982).

[2] D. W. Baker, F. K. Forster, and R. E. Daigle, ''Doppler principles and techniques,'' in *Ultrasound: Its Applications in Medicine and Biology* (Elsevier Scientific, Amsterdam, The Netherlands, 1978), Chap. III, pp. 161–287.

[3] W. D. Barber, J. W. Eberhard, and S. G. Karr, ''A new time domain technique for velocity measurements using Doppler ultrasound,'' IEEE Trans. Biomed. Eng. **32**(3) 213–229 (1985).

[4] J. E. Wilhjelm, ''Quantitative Comparison Between PW-psm and PW-tsm Doppler Systems,'' in Proc. IEEE-UFFC Ultrasonics Symposium, 1281–1284 (December 1991).

[5] O. Bonnefous and P. Pesqué, ''Time domain formulation of pulse Doppler ultrasound and blood velocity estimation by cross-correlation,'' Ultrason. Imag. **8**(1), 73–85 (1986).

[6] D. Dotti *et al.*, ''Blood flow measurements by ultrasound correlation techniques,'' Energ. Nucl. **23**(11), 571–575 (1976).

[7] P. M. Embree and W. D. O'Brien, ''Volumetric blood flow via time-domain correlation: experimental verification,'' IEEE Trans. Ultrason. Ferroelec. Freq. Control **37**(3), 176–189 (1990).

[8] S. G. Foster, P. M. Embree, and W. D. O'Brien, ''Flow velocity profile via time-domain correlation: error analysis and computer simulation,'' IEEE Trans. Ultrason. Ferroelec. Freq. Control **37**(3), 164–175 (1990).

[9] V. L. Newhouse and P. J. Bendick, ''Analysis of random signal blood flow measurement,'' *1973 IEEE Ultrasonics Symposium Proceedings* (IEEE Press, Piscataway, NJ, 1973), pp. 94–97.

[10] V. L. Newhouse, P. J. Bendick, and L. W. Varner, ''Analysis of transit time effects on Doppler flow measurements,'' IEEE Trans. Biomed. Eng. **23**(5), 381–387 (1976).

[11] D. J. Cathignol, ''Signal-to-clutter ratio in pseudo random Doppler flowmeter,'' Ultrason. Imag. **8**(4), 272–284 (1986).

[12] D. J. Cathignol, C. Fourcade, and J-Y. Chapelon, ''Transcutaneous blood flow measurements using pseudorandom noise Doppler system,'' IEEE Trans. Biomed. Eng. **27**, 30–36 (1980).

[13] J. E. Wilhjelm, ''Ultrasound FM Doppler system for flow profiling with comparison to PW Doppler systems,'' PhD thesis, Dept. of Biomed. Eng., Worcester Polytechnic Institute, MA, 1991.

[14] J. E. Wilhjelm and P. C. Pedersen, ''Target Velocity Estimation with FM and PW Echo-Ranging Doppler Systems, Part II—Systems analysis,'' IEEE Trans. Ultrason. Ferroelec. Freq. Control **40**(4), 373–380 (1993).

[15] J. E. Wilhjelm and P. C. Pedersen, ''Target Velocity Estimation with FM and PW Echo-Ranging Doppler Systems, Part I—Signal analysis,'' IEEE Trans. Ultrason. Ferroelec. Freq. Control **40**(4), 366–372 (1993).

[16] F. J. Harris, ''One the use of windows for harmonic analysis with the discrete Fourier transform,'' Proc. IEEE **66**(1), 51–83 (1978).

[17] A. Papoulis, *Signal Analysis* (McGraw-Hill, New York, 1984), Int. ed., Eq. (8-34), p. 273.

[18] J. E. Wilhjelm, ''Bandwidth of Gaussian weighted chirp,'' Electron. Lett. **29**(25), 2161–2162 (1993).

[19] P. C. Pedersen, P. A. Lewin, and L. Bjørnø, ''Application of time delay spectrometry for calibration of ultrasonic transducers,'' IEEE Trans. Ultrason. Ferroelec. Freq. Control **35**(2), 185–205 (1988).

[20] R. E. Ziemer, W. H. Tranter, and D. R. Fannin, *Signals and Systems: Continuous and Discrete* (Macmillan, New York, 1993), pp. 367–371.

[21] D. Y. Goswami, ''Velocity profiles of Liquid Flow through Circular Tubes and how they affect Flow measurement,'' J. Solar Energy Eng. **113**, 206–210 (1991).

[22] I. S. Gradshteyn and I. M. Ryzhik, *Table of Integrals, Series and Products* (Academic, New York, 1983), 4th ed., Eqs. 3.322-2 and 3.323-2.